ARMY RESEARCH LABORATORY

Explicit Finite Element Methodologies for Simulating the Mega-Hertz Plate and the Ballistic Shock Simulator

by Photios P. Papados, Raju R. Namburu, Krishan Bishnoi, and Douglas Templton

ARL-TR-2494 May 2001

The findings in this report are not to be construed as an official Department of the Army position unless so designated by other authorized documents.

Citation of manufacturer's or trade names does not constitute an official endorsement or approval of the use thereof.

Destroy this report when it is no longer needed. Do not return it to the originator.

Army Research Laboratory
Aberdeen Proving Ground, MD 21005-5067

ARL-TR-2494 **May 2001**

Explicit Finite Element Methodologies for Simulating the Mega-Hertz Plate and the Ballistic Shock Simulator

Photios P. Papados and Raju R. Namburu
Computational and Information Sciences Directorate, ARL

Krishan Bishnoi and Douglas Templton
U.S. Army Tank-Automotive Research, Development, and Engineering Center

Abstract

Modern armored vehicles are equipped with a variety of sensitive components on board, such as computers, telecommunication equipment, range finders, and infrared devices. One potential failure to these sensitive electronic components is due to the high frequency shock wave transmitted through the structure due to impact loads. Failure or malfunction of the electronic equipment can severely damage the combat capability of the armored vehicle, even though the crew survives and the vehicle retains its structural integrity after the impact. These impact loads can be from air blast, land mine detonation, or a projectile penetration. A good understanding of the loading functions due to blast, impact, and penetration, and the stress waves transmitted through the complex vehicle structure due to these impulsive loads, facilitates the improved combat capability of the armored vehicle. Advantages of each of the approaches will be presented, including a comparison of numerical simulations with experimental data.

Contents

List of Figures

INTENTIONALLY LEFT BLANK.

List of Tables

INTENTIONALLY LEFT BLANK.

1. Introduction

Numerous experiments have been carried out during the last decade using the ballistic shock simulator in an attempt to characterize and better understand the ballistic shock environment. One set of such experiments is documented in a 1994 U.S. Army Combat Systems Test Activity, Aberdeen Proving Ground, MD, report [1-3]. These experiments ranged from low to high frequency content of the shock spectrum.

The aim of this work was to numerically model the response of the Mega-Hertz plate and the Ballistic Shock Simulator (BSS) subjected to (a) a loading from a high-energy (HE) source and (b) a loading from a single fragment impact.

In recent years, the responses of structures subjected to loading from HE sources in their vicinity have been reported in the literature [4–6]. Numerical approaches for simulating structural response from air blast loads have been addressed by many authors. Limited literature discussing numerical simulations of structural response from fragment loads is available.

A number of finite-element analyses using scalable hardware and software were carried out. The fragments were modeled both explicitly (actual geometric representation) and implicitly, using an "equivalent" loading function. Rate effects are incorporated in the constitutive models used for these analyses. Their importance is addressed in the discussion that follows.

Traditionally, explicit finite element analysis (FEA) codes [7, 8] are needed to analyze structures that fall in the categories just described. Since structural integrity is usually the main issue, Lagrangian FEA codes are employed. The location of impact and the early transient phenomena are of utmost importance because this is when the FEA mesh distorts extensively in regions near the contact. This causes the explicit time integration analysis to reach critical levels, subsequently causing the computation to prematurely terminate (violation of the Courant condition).

The nature of the problem dictates using nonlinear, high-order constitutive models that incorporate strength enhancements due to high loading rates for both the steel target and the impacting fragment. Another important aspect involves placing the fragments at the right impacting location.

The literature offers no standard or unified procedure for simulating fragment impact on a plate or structure. This is partly because the various investigators disagree on the methodology used to transfer the momentum from the fragment to the target. These methodologies mainly include: (a) an explicit definition of the fragments during the analysis with the FEA code determining the

momentum transfer characteristics, (b) the use of an equivalent loading or forcing function (such as a pressure-time history) which approximates the magnitude and nature of the impacting body, and (c) the direct momentum deposition at the appropriate impact location.

There are advantages and disadvantages for each methodology. The advantage of using the explicit fragment modeling method is the simplicity of defining the appropriate input parameters needed for the simulation. No boundary conditions, other than the velocity of the fragments, are needed. Complications arise, however, in the event that the FEA code does not account for special features such as automatic contact. This can result in redefining the mesh with appropriate interfaces that will not allow the interpenetration of the fragments among themselves or with the actual structure. If the FEA code does not have such interfaces, then this option will prove to be very problematic.

The equivalent-fragment method poses a different problem. This approach requires apriori estimation of the momentum transfer to the target body by the analysts. Depending on the method used, apriori knowledge of the depth of penetration is required. The depth of penetration is used to estimate the duration of the momentum transfer. Knowing the overall duration and magnitude of momentum transferred to the target structure, the equivalent pressure-time history can be constructed. This history, however, can be approximated using various pulse shapes (triangular, square, parabolic, exponential, or any combination of these).

2. Mathematical Formulations

2.1 Explicit Finite Element Method

Numerically solving continuum equations proceeds by initially discretizing the space variables using finite element methods that incorporate constitutive equations and failure models. Subsequently, finite difference methods are employed to discretize the time variables. Time discretization schemes are classified as implicit, explicit, and mixed integration methods. The constitutive equations and underlying failure models are based on theoretical and/or empirical models. They vary from purely phenomenological to microstructurally based prediction procedures. Stress waves and shock waves are an important part of the solution for simulating short transient phenomena; hence, the solution is advanced in time using an explicit-time integration scheme. The explicit method, however, is only conditionally stable (i.e., the size of the time step is limited by the Courant stability criteria and is usually very small).

In an explicit time integration procedure, the mass matrix M is lumped. Consequently, the equations can be solved independently from each other, as shown in equations 1-3. Hence, an explicit method is very attractive for vector and parallel computations, and the solution procedure can exploit both shared memory vector and distributed memory multiple processor computers.

$$Ma^n = F^n_{internal} + F^n_{applied} + F^n_{\text{contact}}, \tag{1}$$

$$v^{n+\frac{1}{2}} = v^{n-\frac{1}{2}} + \Delta t a^n, \tag{2}$$

and

$$x^{n+1} = x^n + \Delta t v^{n+\frac{1}{2}}, \tag{3}$$

where x is the displacement, v is the velocity, a is the acceleration, and Δt is the time integration increment or time step. The superscript n indicates the current time level and n+1 indicates the next time level. Nonlinear material constitutive relations are considered in evaluating $F_{internal}$. From a computing point of view, this term is the most expensive in explicit codes. Evaluating $F_{contact}$ involves searching, and hence additional communications are required on scalable computers. ParaDyn is the FEA code used in this study. The following four steps are involved in solving applications using ParaDyn on scalable computers:

(1) mesh/grid generation using preprocessing software [9] with appropriate boundary conditions, initial conditions, and material properties,

(2) partition or spatial decomposition of the solution domain to a desired number of processors [10, 11],

(3) executing the problem on scalable computers, and [12]

(4) gathering and postprocessing results from all the processors [13–15].

Domain decomposition and gathering results are the primary differences between serial and scalable methods. The objective behind partitioning is to balance the computational load and optimize communications between processors. Hoover et al. [12] describe the implementation of ParaDyn on scalable computers.

2.2 Material Constitutive Models

The target was represented using a modified nonlinear, elastic-plastic, rate-dependent constitutive model that was specifically developed for steel [7, 12]. The rate dependency is essential judging from the dynamic and impulsive state of stress that the target is subjected. The explicit modeling of the fragment used a similar material, with the exception that the strength characteristics were

notably different. The HE source was modeled using the default HE material model available in ParaDyn in conjunction with the appropriate equation of state.

2.2.1 Target Constitutive Model

The constitutive model used for the target is an elastic-plastic model with isotropic hardening that accounts for strain rate enhancements and failure considerations of the parent material once a threshold level of strain is reached (Model 24) [7, 8, 12]. The failure criterion is based on the ultimate effective plastic strain accumulation limit provided in advance. The equation governing the effective plastic strain accumulation is

$$\varepsilon_{eff}^{pl} = \int d\varepsilon_{eff}^{pl} \quad \text{and} \quad d\varepsilon_{eff}^{pl} = \sqrt{\frac{2}{3} d\varepsilon^{pl} d\varepsilon^{pl}}, \tag{4}$$

where ε_{eff}^{pl} and ε^{pl} are the effective plastic and plastic strains, respectively. The default constitutive model, found in the original DYNA3D-LLNL, is not suited to provide ultimate strain-level considerations for all types of elements (one-, two-, and three-dimensional elements). Moreover, abrupt elimination of the failed elements produces spurious waves and artificial vibration of the adjacent elements. The modified Model 24 was developed specifically to correct for these needs. Both models account for strain rate enhancements.

2.2.2 Fragment Constitutive Model

The constitutive model used for the fragment steel is attempting to simulate a deforming material model with an excessively high stiffness characteristic. The model is primarily the same as that used for the target, with the exception that erosion attributes were omitted. Rate enhancements were also incorporated in simulating the fragment. Equation 4 applies to the accumulation of plastic strain and, subsequently, the damage characteristics of the impacting structure.

2.3 Fragment Simulations

Two such simulations were carried out using (a) an explicit fragment that is accelerated toward the structure and (b) equivalent pressure time histories to represent the fragment. In all cases, the angle of impact was assumed perpendicular (90°).

2.3.1 Fragments Modeled Explicitly

The geometry of the target structure was modeled in a detailed fashion and is described in subsequent parts of this report.

The analysis involving the explicit representation of the fragment required two iterations, during which the critical time step was obtained and included as a failure criterion for the elements associated with it. The erosion capability was subsequently activated, and the failed material was removed from the active mesh. It should be noted that the nodes of the failed material remain in the computation, thus preserving the original mass of the structure. Momentum is also preserved, but not the total energy. In other words, there is an error associated with solving the weak formulation of the governing equations since the product of the stress related variables and the strain related variables for the case of the eroded elements are zeroed out. The reason for this is because the stress components of the eroded elements are eliminated. One hopes that the total energy of the eroded material is relatively small (within two orders of magnitude lower) compared with the energy of the overall structure.

The through thickness of the target plate has been represented with 6–10 elements, depending on the simulation. In the absence of higher order elements in the FEM code, the through thickness integration increase of elements gives rise to an increase of Gauss-Points. Thus, wave propagation characteristics can be adequately captured.

2.3.2 Evaluating Equivalent Pressure-Time History

The second simulation uses the equivalent pressure-time history approach. This is a conservative estimate of the momentum. It is based on the assumptions that the original momentum is totally deposited onto the structure and that there is no rebound of the fragments. The fragments are considered to be rigid (compared to the target), and no deformation is associated with them. Equation 5 can be used to transform the original momentum into an equivalent pressure-time history.

$$m\,u = \int_0^{\tau} p\,A\;dt, \tag{5}$$

where m and u are the mass and velocity of the fragment prior to impacting the target and p is the equivalent pressure applied over an area A and integrated between the time limits 0 and τ. τ is the duration of the pulse and is dependent on the depth of penetration X_f and the velocity v_i ($v_f = 0$) of the fragment. The penetration of the fragment is known apriori (either from empirical based calculations or physical measurements of the craters), while the velocity is measured during the experiment. These two parameters are used to compute the duration of the fragment acting on the target as follows:

$$\tau = \frac{2X}{v_i - v_f}. \tag{6}$$

Subsequently, the shape of the pulse is assumed (in this case triangular), and the bounds are estimated. For this study, the rise time of the pulse is assumed to be one quarter of the overall pulse. The peak P_{max} is calculated from the area of the triangle and the overall momentum.

$$P_{max} = \frac{2mu}{\tau A}. \tag{7}$$

The reader may notice that the approach for estimating the equivalent pressure-time history is derived primarily from the approach to do so for "hard" impactors on "soft" structures, such as steel fragments on reinforced concrete. In this case, this methodology is appropriate due to the relatively high ratio of fragment to target stiffness.

3. Mega-Hertz Plate Simulation

3.1 Introduction

A single plate (12 ft × 6 ft × 3 in) subjected to a 20-mm fragment with an impact velocity of 4,420 ft/s was tested at the U.S. Army Aberdeen Test Center (ATC), Aberdeen Proving Ground, MD, as described by Walton [2]. Experimental data were collected relating to displacement, velocity, acceleration, and strain histories. The aim of this exercise was to compare the collected data with performed numerical output extracted from FE analyses.

The scheme described in section 2 was used for the numerical analyses, (i.e., both the implicit and explicit methods were attempted, and eventually, the most efficient method was established).

3.2 FEA Details

Three sets of analyses were performed using the equivalent pressure-time history approach. Gradation of mesh discretization was attempted in an effort to study the convergence of the FEM solution. Coarse (31,104), medium (248,832), and fine (1,990,656) mesh arrangements comprised of hexahedral continuum elements were elected to be tested for each aforementioned case, respectively. The number in parentheses indicates the number of elements used for each simulation. In the case of the fine mesh, the analysis task can become very formidable since the FE mesh is substantially large. Compared to an FE analysis

that explicitly defines the fragment, it is still quite favorable since the latter can yield mesh generation requirements that are of an order of magnitude larger than that used for the fine mesh.

The distribution of the three meshes for the coarse, medium, and fine meshes is shown in Figure 1. The coarse mesh was distributed to 4 processors, the medium to 8, and the fine to 32 for the FEA attempted. In the case of the medium mesh, the FEA mesh is superimposed to the processor distribution graph for the sake of illustration. A similar attempt for the fine mesh would yield a nonvisual graph due to the "density" of the element distribution.

In all cases, the initial velocity (velocity of impact) was measured at 4,420 ft/s. The equivalent pressure-time history approach is based on this initial condition.

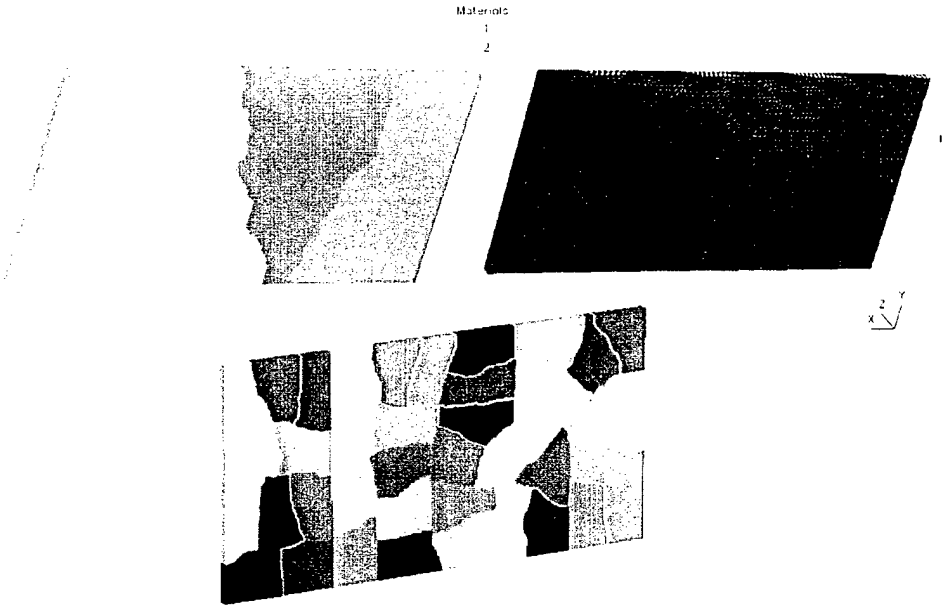

Figure 1. Clockwise from top left: coarse, medium, and fine mesh distributions for 4, 8, and 32 processors, respectively.

3.3 Results

Measurements at several locations were established throughout the experimental work. Gages were mounted at the center, quarter points, and adjacent to the edges of the plate. The results from these locations were directly compared to the FE output.

Figure 2 compares the displacement histories from the three FE analyses performed. It is noted that the displacement characteristic from the medium and the fine meshes compare favorably with each other as well as with the experimental data, although the peak time and value from the fine mesh analysis

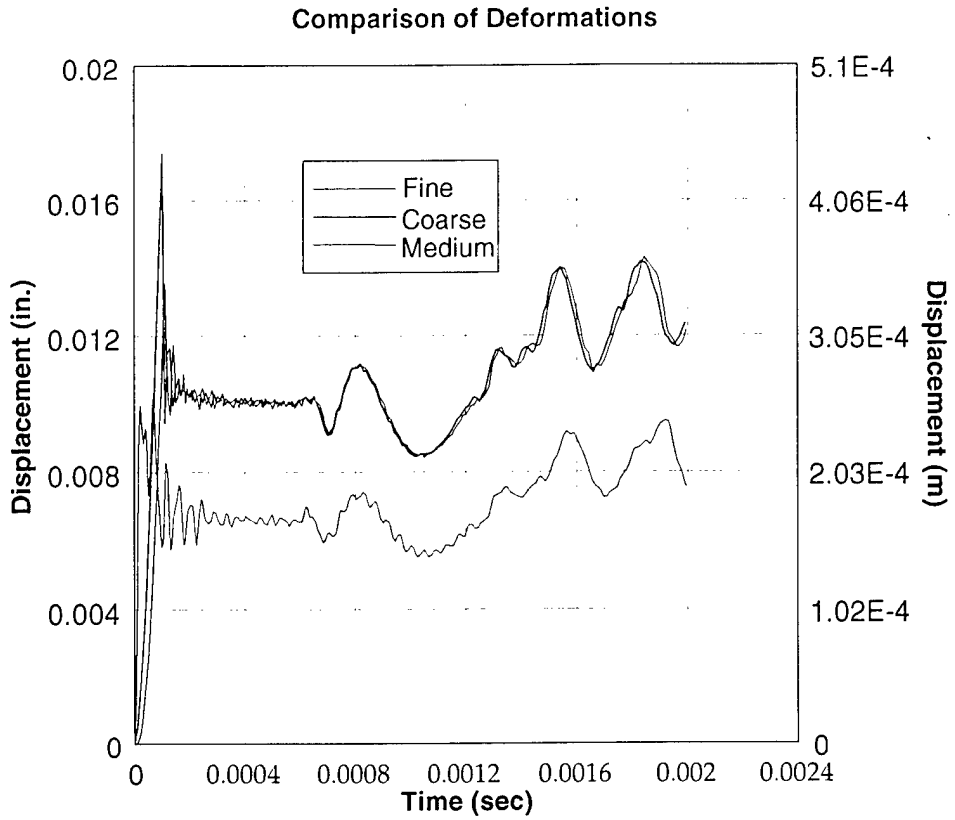

Figure 2. Comparison of displacement responses for the coarse, fine, and medium meshes.

is significantly different (15% higher) from that of the medium mesh. The coarse mesh output does not converge to the displacement levels of the other two shown analyses, although the tracking of the response is proportionally lower. One should wonder as to the benefit of using the fine mesh vs. the medium. The answer becomes apparent later, when the response spectra of the different analyses are compared to the experimental data.

Wave propagation characteristics cannot really be captured by mechanical means since these require a full-field gage distribution, which poses tremendous technical and financial difficulties in implementing. The use of FEA techniques, however, allows us to evaluate the wave propagation phenomena within the continuum under consideration. Selected effective stress outputs are shown for the case of the fine mesh in Figure 3. The progression in time occurs clockwise, starting from the top left corner. The initial ripples shown are due to the fragment impact. They propagate in time until they reach the free surfaces of the structure. Subsequently, they are initially reflected, as shown in the third plot of Figure 3; eventually, they form constructive and destructive waves due to multiple reflections and interactions (last plot).

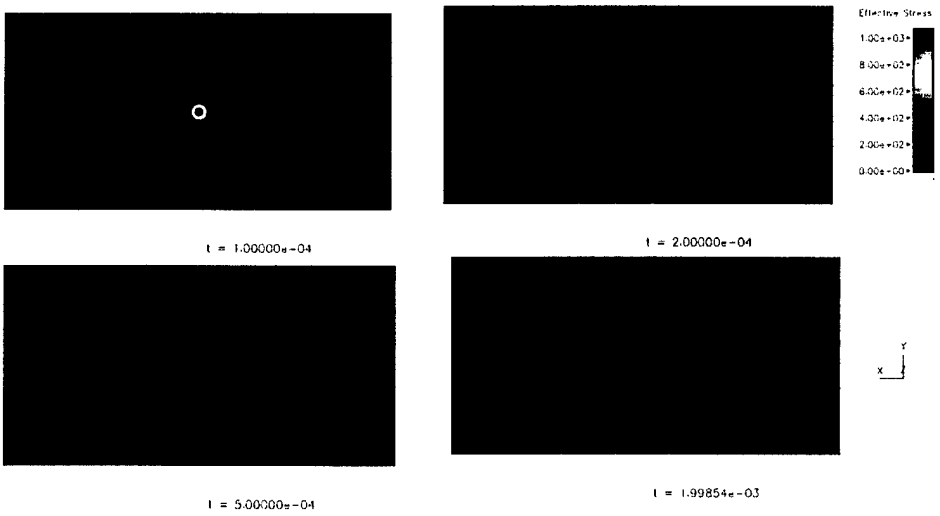

Figure 3. Effective stress output for the fine mesh FEA.

The response spectra from the three FEA and the experimental data are shown in Figure 4. It becomes evident that the fine FEA yields the best results compared to the other two analyses. Although the medium mesh analysis does not yield results that are dramatically different from the experimental, the fidelity of the output is not as high as that of the fine FE analysis.

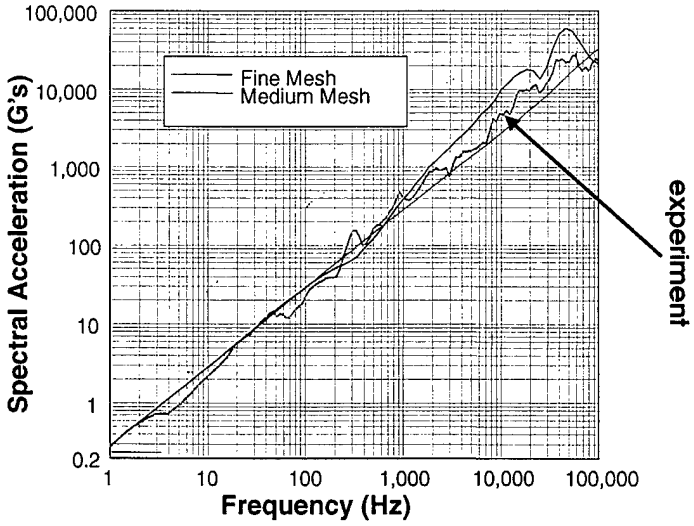

Figure 4. Comparison of response spectra.

4. Ballistic Shock Simulator (BSS) Study

Two cases were studied with respect to the empty BSS [1]. The first one deals with a single fragment (Case I), both explicitly and implicitly modeled, impacting the target; the second case involves a charge (Case II) placed adjacent to the target and detonated to produce a dynamic-impact loading condition.

4.1 Single Fragment Impact-Empty BSS Option

A traditional approach for simulating the 37-mm fragment with an impact velocity of 600 m/s requires the modeling of all parts (i.e., both the target and impact slug). A nontraditional approach involved the development of equivalent pressure-time histories that represent the deposition of momentum from fragments onto the structure under investigation and as explained mathematically in section 2.

4.1.1 Methodology

The geometry of the BSS without the cover (empty option) was numerically modeled using INGRID [9], a preprocessor used in conjunction with the LLNL FEA software [7, 8, 12]. The representation of the structure is shown in Figure 5.

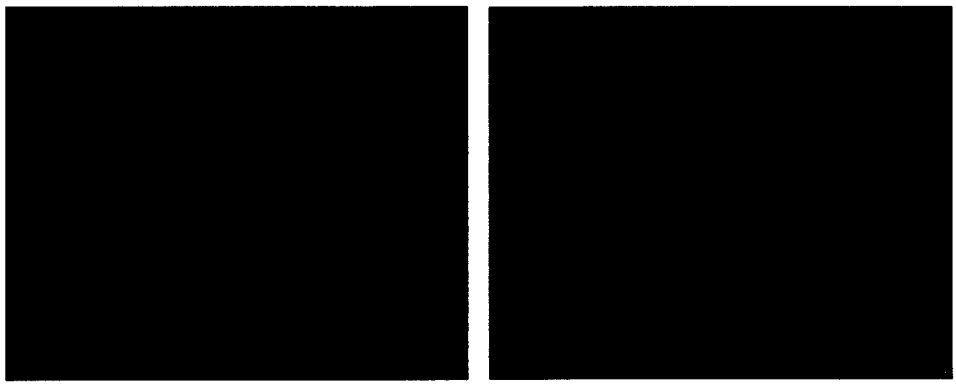

Figure 5. Numerical representation of the BSS structure.

A detailed view of the front (impact) portion of the structure is shown in Figure 6. The plate at the front of the structure represents an impact plate that is expendable, and its sole role is to provide protection to the actual BSS structure. The geometrical details modeled include the access ports and the exact thickness of the plates comprising the overall structure.

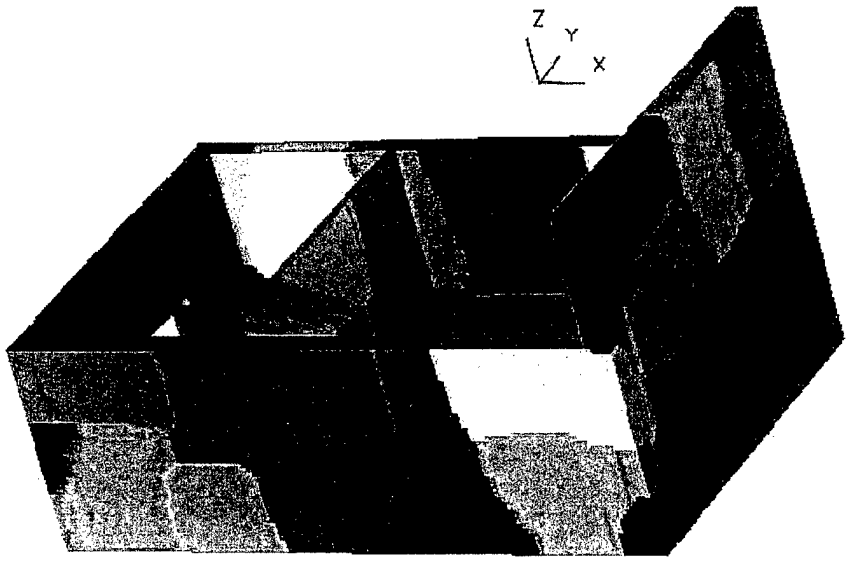

Figure 6. Domain decomposition of the BSS structure—Case I.

The fragment is explicitly modeled. In other words, the geometry of the fragment was replicated in a numerical model with the appropriate material model specifications indicated by Walton [1], as well as the appropriate boundary conditions (initial conditions). In this case, the initial condition is the velocity of the fragment prior to impacting the front plate of the BSS. Strain rate enhancements were used because of the highly dynamic nature of the problem.

What became necessary was an increased mesh size, due to the impact of a small object onto a massive structure. The aim of the exercise was to capture the wave propagation characteristics of the BSS due to this impact. At the same time, the impact-contact region needed special attention, so the transfer of the load/momentum was the appropriate choice. This led to the generation of an FEA model that exceeded 1.5 million elements or the equivalent of approximately 6 million degrees of freedom. Subsequently, the problem was partitioned to 32 processors for the analysis to be carried out. Figure 6 shows the domain decomposition of the problem at hand for the 32 processors.

4.1.2 Results

The simulation time was 5 ms, and the CPU time was in excess of 30 hr. The numerical results indicate that local damage was incurred on the structure which extended approximately 1.5 times the diameter of the impacting fragment. The damage was primarily restricted within the front plate of the overall arrangement. Figure 7 shows a close up of the fragment prior to impact with the

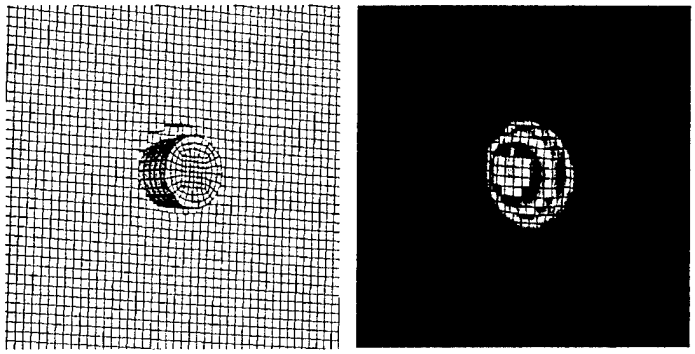

Figure 7. Progressive damage due to impact.

plate, as well as the sequence of events that follow the impact. In the second picture of Figure 7, the impactor shows a significant deformation, while subsequent pictures indicate the partial penetration (damage) of the plate. The last picture shows the formed crater while the impactor bounced back (not shown). Through the eroded elements, the analysis indicates the scale of damage incurred. The actual experiment yielded similar results according to Walton [1]. It is believed that the BSS structure remains well within the elastic range with no apparent damage, except for the front plate as discussed earlier.

A substantial reduction in CPU and thus the turnaround time is accomplished if one uses the equivalent pressure-time load (EPL) history approach. The mesh size can be reduced to approximately 50% of the original size with no apparent deviation in the numerical results.

The reason is due to the FEA density in the vicinity of the impact that does not need to be of extremely high refinement to capture the impact-contact characteristics of the problem. Even if the mesh is not reduced, the CPU time is still reduced by not less than 60%.

The distribution of the pressure and the wave propagation characteristics of this problem are shown in Figure 8. The local damage is observed once again at the

Figure 8. Pressure distribution for Case I.

center of the plate, and the ripples indicating the wave patterns at this particular instance show how the pressure patterns are distributed through the different portions of the structure.

The actual numerical results are extremely close to the FEA results, as one would expect. The reason is that the overall structure remains elastic, as mentioned earlier, with a slight area of plastification in the vicinity of the impact-contact region. The numerical and experimental peak values are compared in Table 1. It should be noted that two experiments were carried out for this particular configuration. The experimental data are consistent in both cases, except for the strain levels for the back plate. The authors believe that this is due to either gage calibration problems, or most likely to a slightly different position of impact. The latter appears to affect mostly the posterior portion of the BSS structure, as will be observed in a later case study.

4.2 Explosive Part Discussion

4.2.1 Methodology

A novel method is employed in this study concerning the definition, characteristics, and load derivation from the detonation of explosive material. Traditional methods include the definition of the HE source in an explicit fashion, and its subsequent detonation or derivation of equivalent pressure-time histories to represent the yield of the detonated explosive. The former method provides the appropriate environment where both disruptions in pressure and

Table 1. Comparison of experimental and numerical peak values.

Parameter	Event	Front Plate	Middle Plate	Back Plate
Displacement	Experiment	N.A.[a]	N.A.	380, 360
(μm)	FE Analysis	N.A.	N.A.	433
Velocity	Experiment	1.40, 1.10	1.10, 0.90	0.43, 0.41
(m/s)	FE Analysis	1.20	1.06	0.51
Acceleration	Experiment	371, 353	195, 180	312, 308
(g's)	FE Analysis	392	179	318
Strain	Experiment	304, 121	79, 30	56, 15
(μm/m)	FE Analysis	303	81	60

[a]N.A. denotes experimental data not available.

velocity are present; thus, the definition of the shock is more reliable. The latter method provides only the pressure-time dependant condition of the shock, which is accurate only when the explosive is substantially away from the structure under consideration.

Figure 9 shows a bidirectionally constrained explosive material. This FEA model represents a homogeneous isotropic medium surrounding the explosive. Only one-fourth of the actual structure is simulated, although the analyst can perform this task using only one-eighth of the overall structure. The explosive used in this case is the numerical equivalent of C-4 explosive. The shape of the explosive is cylindrical, while that of the adjacent structure is rectangular. The reason for this geometrical representation is that no node correspondence is desired between the explosive and the host structure. The numerical results from this analysis are very limited in terms of the simulation. The reason for this is that the FEA terminated prematurely since the HE source resulted in inverting adjacent FEA elements. This created a negative Jacobian matrix, consequently leading to a violation of the Courant criterion.

In order for this analysis to be successful, the analyst needs to continually delete badly deformed elements via restart operations or use artificial stabilization techniques in an effort to maintain a logical integration time step which satisfies the proper local and global stability conditions.

A remedy to this problem can be introduced by "collapsing" the original explosive charge in two out of the three orthogonal coordinates and by assigning the proper "scaled" properties (Figure 10). The initiation time and location of

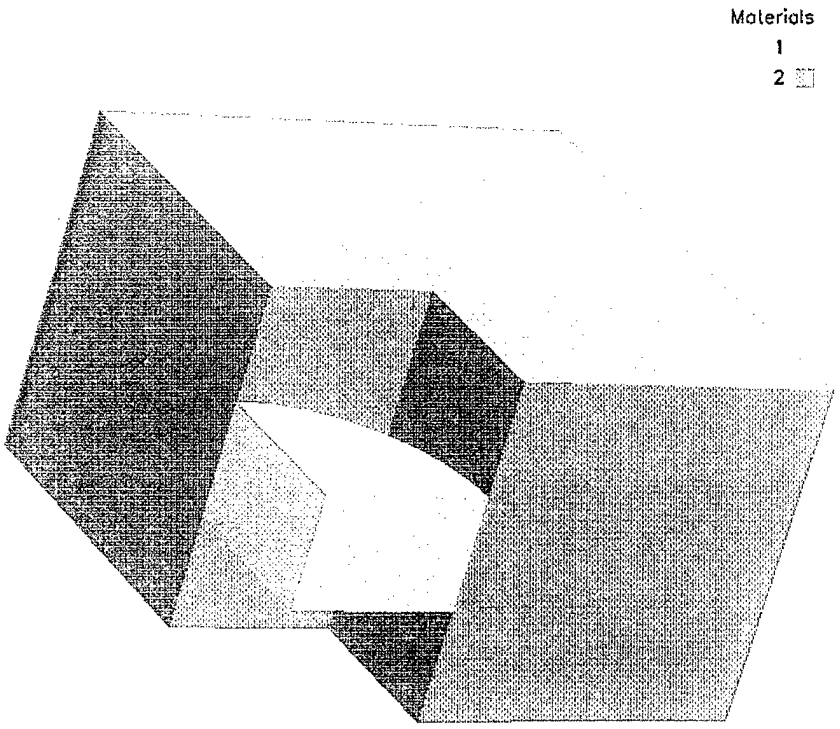

Figure 9. Bidirectionally confined explosive.

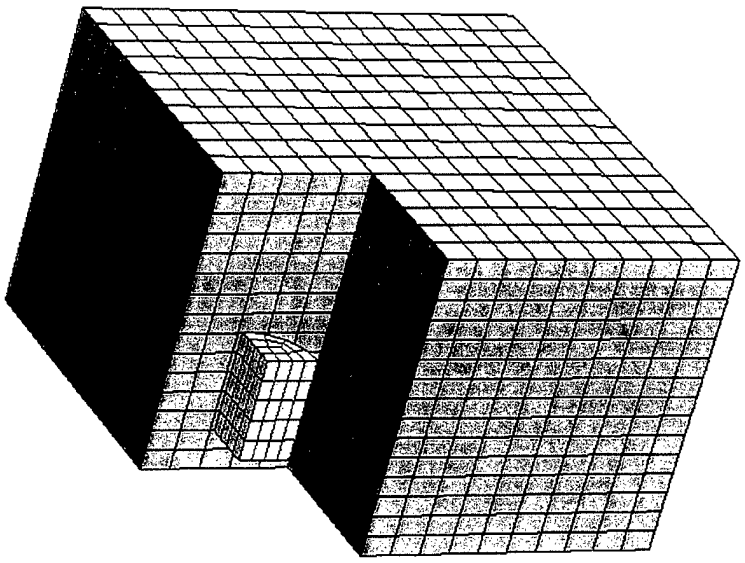

Figure 10. Collapsed explosive representation.

the detonation are not affected. Subsequently, the numerical method used is otherwise identical to that employed with the original charge configuration, as described in the Dyna3d and ParaDyn manuals.

As indicated in Figure 11, this was intended to be a top-down detonation, with the initiation point at the center of the top surface of the explosive. The application of the load due to the detonation on the explosive arrives at the exposed surfaces at precisely the exact time that it would had the original shape of the explosive been preserved. The second picture of Figure 11 shows the deformed state of the explosive, but more importantly it shows the already damaged surfaces of the structure and the extra space created by the eroded elements. The third picture shows an even more advanced stage in the calculation with substantially more damage on the structure. Finally, the last picture shows the final state of the structure with the explosive visually removed to expose the overall effect of the explosive.

4.2.2 Fidelity of the Collapsed Explosive Option (CEO)

The fidelity of the methodology was tested for various explosive charge sizes. The pressure-time history of various elements at various locations on the structure under consideration was compared to the pressure-time derived from the original explosive charge. The results were deemed identical. Due to the short duration of the latter data, the exercise was repeated with an equivalent explosive structure which was geometrically intermediate between the original HE source and the source used in this study.

The five locations shown in this case are all a strand of elements situated adjacent to the left hand side plane of symmetry and at approximately mid-height. The signature of the pressure-time histories is shown graphically in Figure 12. As indicated by this graph, the resulting variable histories are exactly the same in both cases.

Another important issue that arises with this methodology is that of scalability. In the case that the HE is modeled according to its original geometrical dimensions, the CPU time, even for a short duration simulation, is excessive. It requires constant manipulation of the mesh with element deletion, and the overall CPU time increases dramatically. The fact that the Lagrangian mesh deforms excessively in conjunction with the interface contact between the explosive and the structure causes the time step to decrease to levels where the calculation is not practical. The communication time is increased, and the overhead is increased. All of these factors contribute to the scalability of the overall problem not to be preserved.

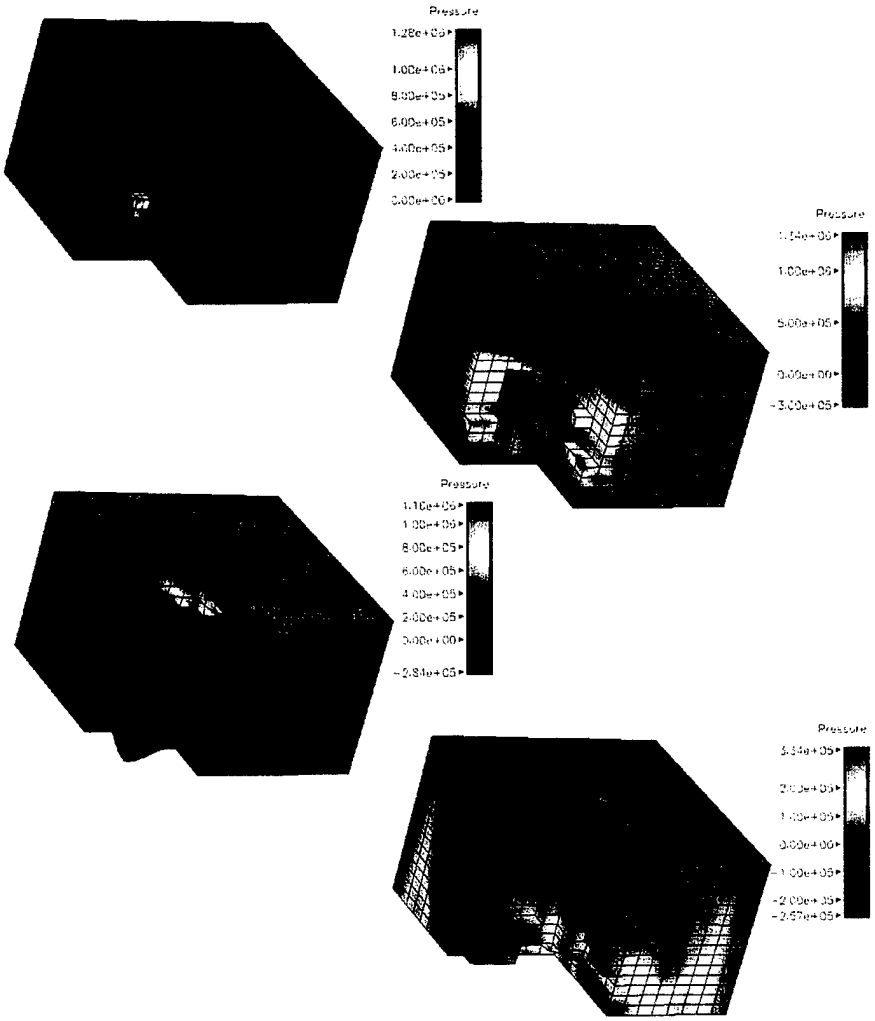

Figure 11. Collapsed explosive option with erosion capability at different stages of the FEA simulation.

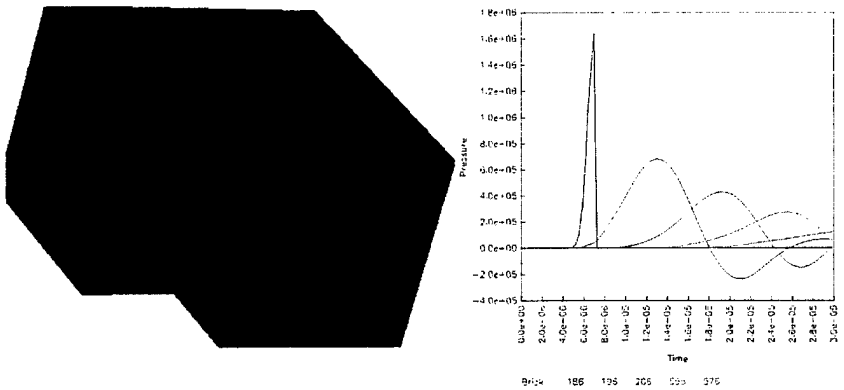

Figure 12. Element arrangement and extracted pressure-time histories.

This issue is eliminated, however, if the CEO approach is used. The contact region is eliminated from the problem (initially at least), excessive deformations are not observed, the time step does not reach critical levels and restart operations become unnecessary. The overall turnaround time is 8 to 10 times faster with the CEO method vs. the traditional approach. Most importantly, the CEO method yields results of a time span that is comparable to those obtained from experimental studies, while the traditional method fails to do so.

4.3 BSS Empty Option—Case II

4.3.1 Methodology

The compressed explosive option (CEO) is used in this case. This methodology is described in section 4.2. The problem was carried out to 10 ms of simulation time, which is substantially more that than of the experimental output available. Once again, the BSS structure does not have the cover plate (empty option).

The properties and nature of the explosive charge (35 g) were not available. The analysts assumed that the explosive under consideration was a C4 charge type. The appropriate material model (material model for high explosives) was used within the FEA code ParaDyn, in conjunction with a WJL equation of state. The material characteristics for this explosive are readily available in the literature and U.S. government reports. Because the numerical and experimental data agree to a considerable degree, the analyst believes that either indeed a C4 charge was used, or at least an explosive that resembles the material characteristics of the C4 was used.

The FEA model used was the same as that used for Case I, except that the impactor was substituted with the HE source. The HE source was center detonated, which is again another assumption that could not be verified one 100%.

4.3.2 Results

Figure 13 shows the progression of the structural response for the BSS in conjunction with the pressure distribution for this particular case. The response is purely elastic, and the output shown in this figure has been magnified by a factor of 50 to provide a significant visual variability. The structure vibrates after the initial shock is delivered, close to its natural frequency. The response is dominated primarily by the first two modal shapes, as described by Walton [1] and as verified independently by the current study.

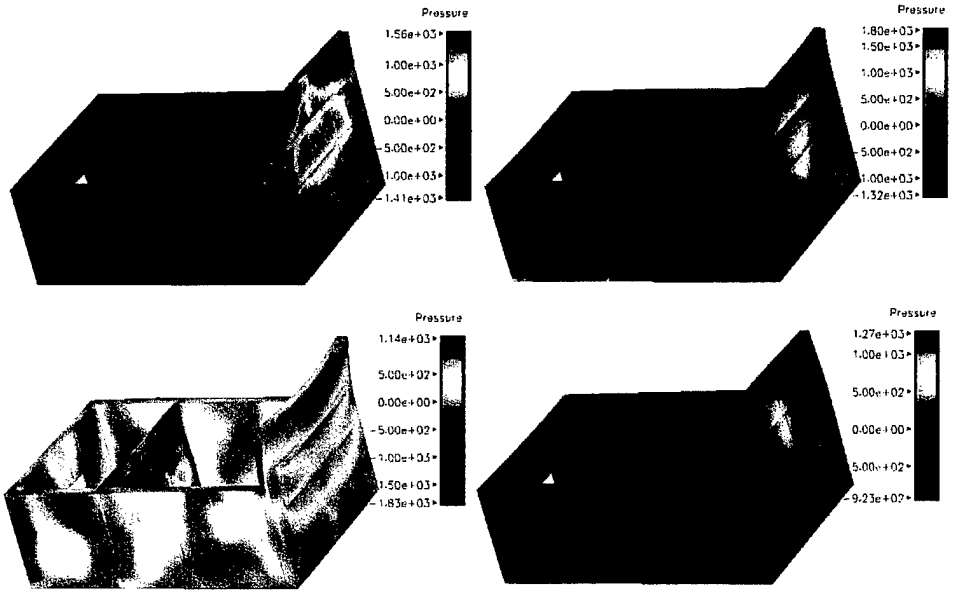

Figure 13. Response shapes and pressure output due to HE source A.

Although deformation plots are not shown for the sake of space, an animation of the response of the BSS structure for this particular case is made available in a soft format for the sake of completeness. The animation is titled "bss_anim_caseII_def.avi," and it is included with the accompanied CD.*

This problem was attempted using the "traditional" explosive method for comparison with the CEO method. The FEA was carried out for a different number of processes in order to address the scalability and effectiveness of each of the methodologies. The results are shown in Figure 14. For the reasons explained in section 4.2 of this report, it is apparent that scalability is not preserved with the traditional method.

Numerical and experimental output were compared for different locations on the BSS structure. Table 2 summarizes the findings from this comparison. All results compare favorably. The only exception to this statement is the comparison of the strain levels at these locations. Once again, the experimental output between the two attempts disagrees as to the strain levels obtained. The FEA strain peak levels appear to agree with the upper range of the measured strains (i.e., compare favorably with experiment 1 but not with experiment 2).

*The CD is available only upon request. Please send all requests to photios@arl.army.mil.

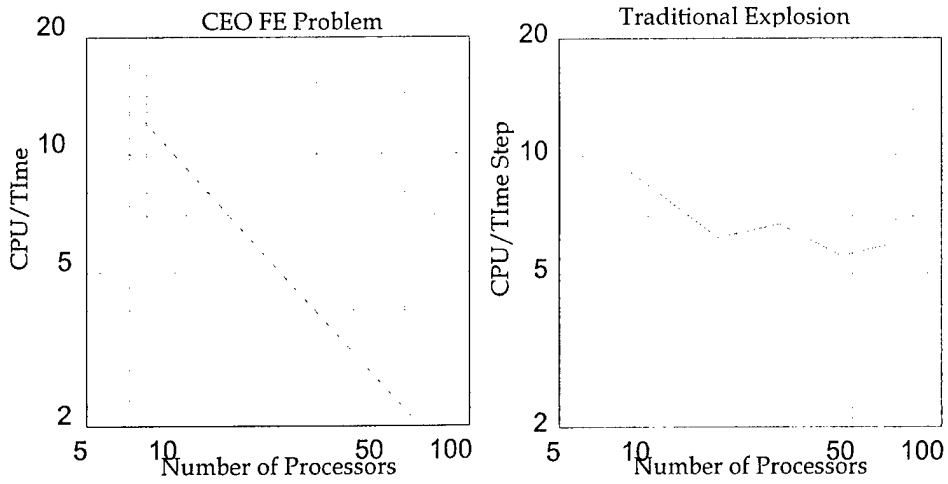

Figure 14. Scalability study for the CEO and traditional modeling methods.

Table 2. Comparison of experimental and numerical peak values.

Parameter	Event	Front Plate	Middle Plate	Back Plate
Displacement	Experiment	N.A.[a]	N.A.[a]	105, 92
(μm)	FE Analysis	673	122	109
Velocity	Experiment	2.26, 2.02	0.34, 0.38	0.30, 0.29
(m/s)	FE Analysis	2.52	0.32	0.33
Acceleration	Experiment	69, 64	54, 62	58, 51
(g's)	FE Analysis	74	60	56
Strain	Experiment	160, 24	58, 6	24, 3
(μm/m)	FE Analysis	78	59	33

[a]N.A. denotes experimental data not available.

5. High-Energy Source Loading for Full Ballistic Shock Simulator: Collapsed Explosive Option

5.1 Methodology

The geometry of the BSS [1] with the cover (full option) was numerically modeled using INGRID [9], as it was done with the empty option of this study. The representation of the structure is shown in Figure 15.

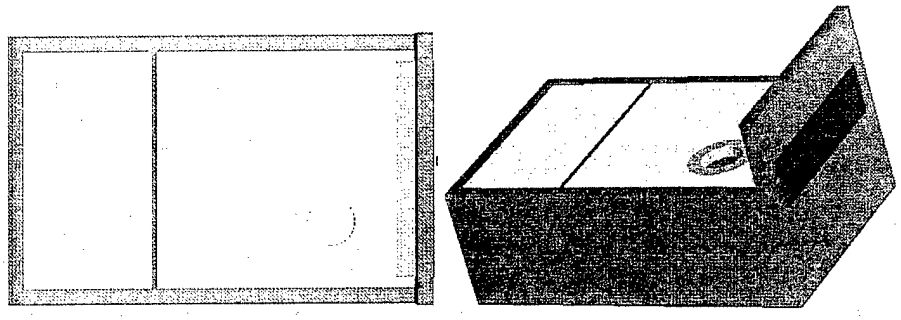

Figure 15. Numerical representation of the BSS structure: full option.

The numerical model compares to that of Figure 1, with the exception that the cover plate has been added. Additional detail of this structure is shown in Figure 16. A zoom-in section of the front plate is shown in the first of the two pictures in Figure 16. The plate at the front of the structure represents an impact plate that is expendable, and its sole role is to provide protection to the actual BSS structure. The geometrical details modeled include the access ports and the exact thickness of the plates comprising the overall structure. In addition, the porthole of the cover plate was modeled to the precise specifications of the blueprint drawings provided to the analyst. Mesh refinement was necessary in this region to avoid specification of tied interfaces. The main disadvantage of using tied interfaces is that it can create spurious waves in the vicinity by trapping and rebounding the waves that arrive in the area of the interface. In a problem such as this, where wave propagation is the main issue, such discrepancies can lead to inexplicable errors.

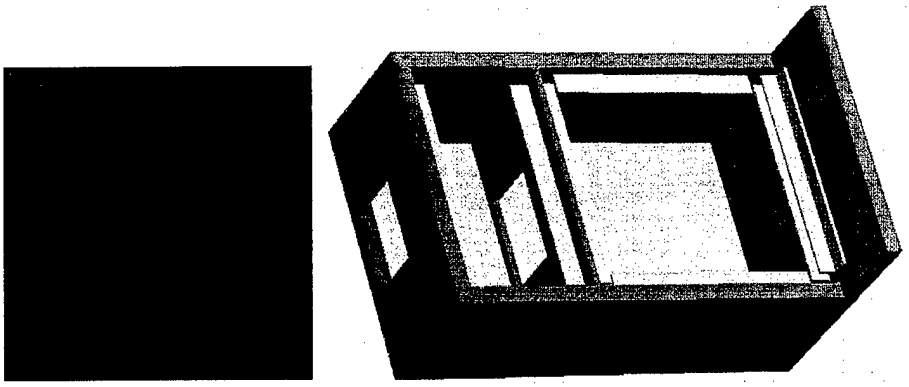

Figure 16. Geometry and mesh details of the BSS structure: full option.

The second picture of Figure 16 shows the added C-channels necessary to support the cover plates. These channels are rigidly attached to the main frame (side plates). In reality, these channels are welded to the main frame. The FEA

model could have been done in such a way to exactly simulate these connections. Due to the added detail, the size of the mesh would have had to increase substantially. This would generate to a mesh that would have been impractical to run. Thus, the approximation of connecting the channels to the main frame was used. Once again, there is no interface between the C-channels and the plates, since the nodal geometry at these locations coincides exactly for the different geometric parts. Thus, a simple tolerance of the common nodes yields a mesh with no added complexity. The same mentality is used for the bolted connections as well. In other words, the bolded connections are assumed to provide a fixed connection at the areas of interest.

The simulation time was 5 ms, and the CPU time was in excess of 17 hr using 64 processors of the Origin 2000 machine. The numerical results indicate that local damage was incurred on the structure which extended approximately along the length of the explosive structure. The damage was primarily restricted within the front plate of the overall arrangement.

5.2 Results

Since the only variable that changed was the overall mass of the structure, which was substantially greater than the one reported in Case II, it is no surprise that the structure retains its elastic response characteristics. The duration of the dynamic effects is slightly shorter than that reported earlier for Case II.

Numerical and experimental output were compared for different locations on the BSS structure. Table 3 summarizes the findings from this comparison. All results compare favorably, although the numerical analysis appears to favor the upper end of the reported experimental output. The strain levels agree between the two experiments, except for the gage reading of the back plate. The FEA appears to report higher values for all strain gages. Velocity values are slightly higher as well. The general correlation between experimental and numerical data is deemed very satisfactory.

Although not shown, scalability for this particular application is preserved. This was studied for only two cases, the 32- and the 64-processor calculations. Since there are no interfaces involved in any of these calculations, there is no reason for scalability not to be preserved, except for the case when the explosive overtakes the structure (gases from the explosive contact the major portion of the structure). At this point, the interface contact problem controls the time step of the computation and the CPU time is necessarily increased.

Table 3. Comparison of experimental and numerical peak values.

Parameter	Event	Front Plate	Middle Plate	Back Plate
Displacement	Experiment	N.A.[a]	70, 65	N.A.[a]
(μm)	FE Analysis	N.A.[a]	62	N.A.[a]
Velocity	Experiment	0.88, 0.82	0.21, 0.18	0.11, 0.12
(m/s)	FE Analysis	0.84	0.25	0.17
Acceleration	Experiment	42, 44	62, 64	14, 15
(g's)	FE Analysis	55	68	16
Strain	Experiment	15, 15	2, 2	20, 11
(μm/m)	FE Analysis	22	14	39

[a] N.A. denotes experimental data not available.

6. Conclusions

Sophisticated models and techniques were carried out in an effort to replicate experimental outcome pertaining to the response of a steel plate target subjected to impact loads due to a fragment. The FEA include the use of both explicit and implicit representation of the fragment. They resort to element elimination techniques such as erosion for removing extensively distorted continuum elements. In the case of the explicit fragments, automatic contact algorithms were used for the interaction of the latter with the target [16–18]. Although bound by simplified assumptions, the equivalent pressure-time loading FEA approach yielded results as promising as the more elaborate explicit technique.

The analyses were performed using serial and scalable software and hardware [19]. The advantage of using a parallel machine vs. a serial one for this type of a problem is shown by the tremendous increase in speed and turnaround times obtained when comparing the two.

Engineering tools such as the code WAVE were used to predict the response spectra of the back plate of the BSS. The comparisons between this code and the actual experimental results are shown in Figure 17. The experimental data are represented by the jagged line, while the two other lines (light and heavy solid lines) are the outcome from the code WAVE with two different loading functions

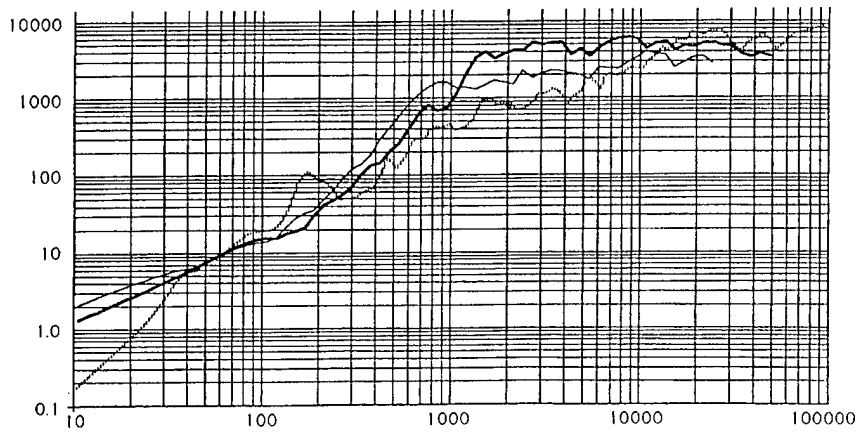

Figure 17. Comparison of acceleration response spectra between experimental and the engineering code WAVE output.

that represent the impulse of the fragment onto the BSS structure. It is evident that there is a large disparity between the experimental and engineering tool outputs.

Figure 18 shows the FEA output response spectra for both the charge weight A and the fragment impact simulation. These spectra compare quite favorably with the experimental spectra shown in Figure 17. Due to the unavailability of the experimental date in a soft format, response spectra from the FEA and the experiment were not merged into a single graph.

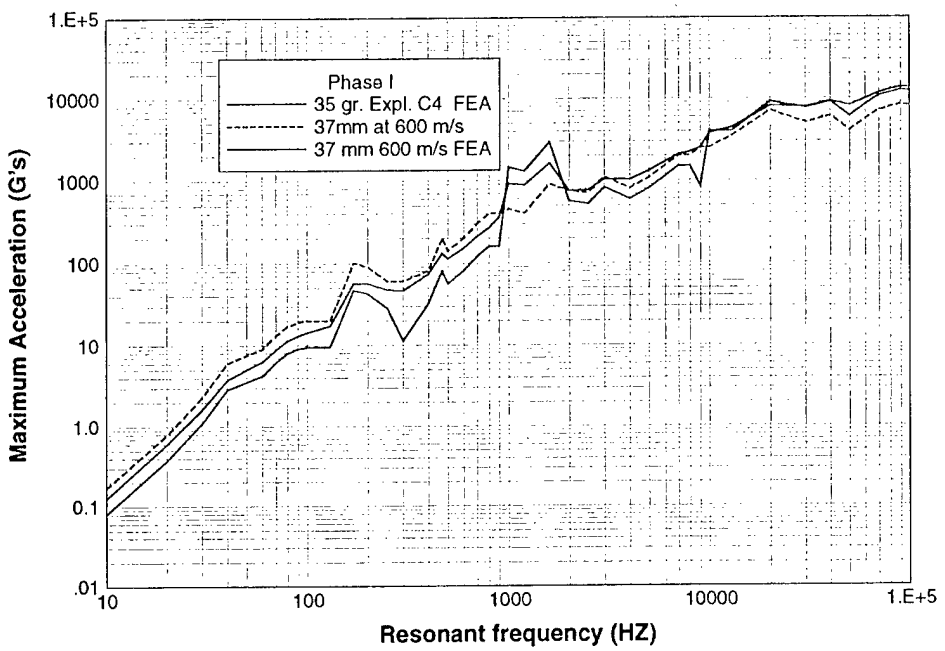

Figure 18. Comparison of acceleration response spectra between experimental and numerical FEA output.

7. References

1. Walton, W. S. "Development of Ballistic Shock Simulators." Report CSTA-7580, U.S. Army Combat Systems Test Activity, Aberdeen Proving Ground, MD, 1994.
2. Walton, W. S. "MHz Plate Data." Data Package CSTA-6262, U.S. Army Combat Systems Test Activity, Aberdeen Proving Ground, MD, 1989.
3. Walton, W. S. "Characteristics of Ballistic Shock." Report CSTA-6262, U.S. Army Combat Systems Test Activity, Aberdeen Proving Ground, MD, 1985.
4. Papados, P. P. "A Reinforced Concrete Structure Under Impact: Response to High Rate Loads." *Structures Under Shock and Impact Loads VI*, Wessex Institute of Technology: WIT Press, 2000.
5. Papados, P. P., and R. R. Namburu. "Simulation of an Imbedded Detonation." Presentation at the 5th International Conference on Structures Under Shock and Impact, Thessaloniki, Greece, 1998.
6. Papados, P. P. "Buried Hardened Structure Response to Airblast and Fragment Loadings From an Internal Detonation." Highlights in Computational Science and Engineering, U.S. Army Engineer Waterways Experiment Station, Special Report, Vicksburg, MS, 1998.
7. Whirley, R. G., and B. E. Engelmann. *DYNA3D – a Nonlinear Explicit, Three-Dimensional Finite Element Code for Solid and Structural Mechanics - Users Manual.* UCRL-MA-107254, rev. 1, Lawrence Livermore National Laboratory, Livermore, CA, 1993.
8. Hoover, G. G., A. J. DeGroot, J. D. Maltby, and R. J. Procassini. *PARADYN - DYNA3D for Massively Parallel Computers. Engineering Research.* UCRL 53868-94, Development and Technology FY94, Lawrence Livermore National Laboratory, Livermore, CA, 1995.
9. Christon, M. A., and D. Dovey. *INGRID User Manual. A 3-D Mesh Generator for Modeling Nonlinear Systems.* Originated by D. W. Stillman, J. O. Hallquist, and R. R. Rainsberger. Methods Development Group, Lawrence Livermore National Laboratory, Draft, Livermore, CA, 1992.
10. Karypis, G., and V. Kumar. "A Fast and High Quality Multilevel Scheme for Partitioning Irregular Graphs." TR 95-035, Department of Computer Science, University of Minnesota, Minneapolis, MN, 1995.

11. Procassini, R. J., A. J. DeGroot, and J. D. Maltby. *PartMesh User Manual-Partitioning Unstructured Finite Element Meshes for Solution on a Massively Parallel Processor.* UCRL-MA-118774, Methods Development Group, Mechanical Engineering, Lawrence Livermore National Laboratory, Livermore, CA, 1994.

12. Hoover, G. G., J. A. DeGroot, and R. J. Sherwood. *ParaDyn: A Parallel, Nonlinear, Explicit, Three-Dimensional Finite-Element Code for Solid and Structural Mechanics. User Manual.* Methods Development Group, Lawrence Livermore National Laboratory, Draft: ParaDyn Version 1.01, Livermore, CA, 2000.

13. Procassini, R. J., and A. J. DeGroot. *CombinePlt and CombineThs User Manual.* UCRL-MA-121327, Methods Development Group, Lawrence Livermore National Laboratory, Livermore, CA, 1995.

14. Dovey, D., and T. E. Spelce. *GRIZ: Finite Element Analysis Results Visualization for Unstructured Grids. User Manual.* UCRL-MA-115696, Methods Development Group, Lawrence Livermore National Laboratory, Livermore, CA, 1996.

15. Spelce, D. E. *THUG: Time Histories from Unstructured Grids. User Manual.* Methods Development Group, Lawrence Livermore National Laboratory, Draft, Livermore, CA, 1996.

16. Papados, P. P. "Solving Military Problems Using High-Performance Tools." MABS 16, Military Aspects of Blast and Shock, Oxford, England, 2000.

17. Papados, P. P., and R. R. Namburu. "Simulation of Single and Multiple Fragments Impacting an RC Slab." Ninth International Symposium Interaction of the Effects of Munitions With Structures, Berlin, Germany, 1999.

18. Papados, P. P., R. R. Namburu, and C. Bishnoi. "Fragment Impact on a Plate." Presentation, abstract in Proceedings of USACM, United States Association for Computational Mechanics, Boulder, CO, 1999.

19. Papados, P. P., and T. L. Bevins. "Numerical Simulation of a Complex Structure Using Scalable Hardware and Software." IMPLAST 2000, Melbourne, Australia, 2000.

List of Symbols

Unless stated otherwise, all indices vary according to dimensionality of the problem, e.g., n = 1, 2, 3 in a three-dimensional structure.

a	Acceleration vector
A	Area of contact of fragment with target
$F_{internal}$	Internal forces vector
$F_{applied}$	Applied forces vector
$F_{contact}$	Contact forces vector
m	Mass of fragment
M	Mass matrix
P_{max}	Peak pressure
u	Velocity of fragment
p	Pressure
v	Velocity vector
v_f , v_i	Final and initial velocities of a fragment
x	Displacement vector
X_f	Depth of penetration
Δt	Time increment
ε_{eff}^{pl}	Effective plastic strain tensor
ε^{pl}	Plastic strain tensor
τ	Duration of pulse

INTENTIONALLY LEFT BLANK.

NO. OF COPIES	ORGANIZATION
2	DEFENSE TECHNICAL INFORMATION CENTER DTIC OCA 8725 JOHN J KINGMAN RD STE 0944 FT BELVOIR VA 22060-6218
1	HQDA DAMO FDT 400 ARMY PENTAGON WASHINGTON DC 20310-0460
1	OSD OUSD(A&T)/ODDR&E(R) DR R J TREW 3800 DEFENSE PENTAGON WASHINGTON DC 20301-3800
1	COMMANDING GENERAL US ARMY MATERIEL CMD AMCRDA TF 5001 EISENHOWER AVE ALEXANDRIA VA 22333-0001
1	INST FOR ADVNCD TCHNLGY THE UNIV OF TEXAS AT AUSTIN 3925 W BRAKER LN STE 400 AUSTIN TX 78759-5316
1	DARPA SPECIAL PROJECTS OFFICE J CARLINI 3701 N FAIRFAX DR ARLINGTON VA 22203-1714
1	US MILITARY ACADEMY MATH SCI CTR EXCELLENCE MADN MATH MAJ HUBER THAYER HALL WEST POINT NY 10996-1786
1	DIRECTOR US ARMY RESEARCH LAB AMSRL D DR D SMITH 2800 POWDER MILL RD ADELPHI MD 20783-1197

NO. OF COPIES	ORGANIZATION
1	DIRECTOR US ARMY RESEARCH LAB AMSRL CI AI R 2800 POWDER MILL RD ADELPHI MD 20783-1197
3	DIRECTOR US ARMY RESEARCH LAB AMSRL CI LL 2800 POWDER MILL RD ADELPHI MD 20783-1197
3	DIRECTOR US ARMY RESEARCH LAB AMSRL CI IS T 2800 POWDER MILL RD ADELPHI MD 20783-1197
	ABERDEEN PROVING GROUND
2	DIR USARL AMSRL CI LP (BLDG 305)

NO. OF COPIES	ORGANIZATION
1	DIRECTOR US ARMY RESEARCH LAB AMSRL CP CA D SNIDER 2800 POWDER MILL RD ADELPHI MD 20783-1145
1	DIRECTOR DA OASARDA SARD SO 103 ARMY PENTAGON WASHINGTON DC 20310-0103
1	COMMANDER US ARMY MATERIAL CMD AMXMI INT 5001 EISENHOWER AVE ALEXANDRIA VA 22333-0001
1	DEPUTY ASST SCY FOR R&T SARD TT RM 3EA79 THE PENTAGON WASHINGTON DC 20301-7100
3	COMMANDER US ARMY TACOM PM TACTICAL VEHICLES SFAE TVL SFAE TVM SFAE TVH 6501 ELEVEN MILE RD WARREN MI 48397-5000
1	COMMANDER US ARMY TACOM PM TACTICAL VEHICLES PM RDT&E 6501 ELEVEN MILE RD WARREN MI 48397-5000
1	COMMANDER US ARMY TACOM PM TACTICAL SURVIVABLE SYSTEMS SFAE GCSS W GSI H 6501 ELEVEN MILE RD WARREN MI 48397-5000

NO. OF COPIES	ORGANIZATION
5	COMMANDER US ARMY TACOM ASMTA TR R J CHAPIN R MCCLELLAND J FLORENCE J THOMSON K BISHNOI 6501 ELEVEN MILE RD WARREN MI 48397-5000
	ABERDEEN PROVING GROUND
24	DIR USARL AMSRL CI H C NIETUBICZ AMSRL CI HC A MARK R NAMBURU P PAPADOS (20 CPS) AMSRL WM TC K KIMSEY

REPORT DOCUMENTATION PAGE

Form Approved
OMB No. 0704-0188

1. AGENCY USE ONLY *(Leave blank)*	2. REPORT DATE	3. REPORT TYPE AND DATES COVERED
	May 2001	Final, Sep 00 - Apr 01

4. TITLE AND SUBTITLE
Explicit Finite Element Methodologies for Simulating the Mega-Hertz Plate and the Ballistic Shock Simulator

5. FUNDING NUMBERS
66260C05/665803.731

6. AUTHOR(S)
Photios P. Papados, Raju R. Namburu, Krishan Bishnoi,*
and Douglas Templton*

7. PERFORMING ORGANIZATION NAME(S) AND ADDRESS(ES)
U.S. Army Research Laboratory
ATTN: AMSRL-CI-HC
Aberdeen Proving Ground, MD 21005-5067

8. PERFORMING ORGANIZATION REPORT NUMBER
ARL-TR-2494

9. SPONSORING/MONITORING AGENCY NAMES(S) AND ADDRESS(ES)
U.S. Army Tank-Automotive Research, Development, and Engineering Center
6501 Eleven Mile Road
Warren, MI 48397-5000

10.SPONSORING/MONITORING AGENCY REPORT NUMBER

11. SUPPLEMENTARY NOTES
*U.S. Army Tank-Automotive Research, Development, and Engineering Center, 6501 Eleven Mile Road, Warrren, MI 48397-5000

12a. DISTRIBUTION/AVAILABILITY STATEMENT
Approved for public release; distribution is unlimited.

12b. DISTRIBUTION CODE

13. ABSTRACT*(Maximum 200 words)*

Modern armored vehicles are equipped with a variety of sensitive components on board, such as computers, telecommunication equipment, range finders, and infrared devices. One potential failure to these sensitive electronic components is due to the high frequency shock wave transmitted through the structure due to impact loads. Failure or malfunction of the electronic equipment can severely damage the combat capability of the armored vehicle, even though the crew survives and the vehicle retains its structural integrity after the impact. These impact loads can be from air blast, land mine detonation, or a projectile penetration. A good understanding of the loading functions due to blast, impact, and penetration, and the stress waves transmitted through the complex vehicle structure due to these impulsive loads, facilitates the improved combat capability of the armored vehicle. Advantages of each of the approaches will be presented, including a comparison of numerical simulations with experimental data.

14. SUBJECT TERMS	15. NUMBER OF PAGES
high frequency, response spectra, FE, BSS, dynamic loads, HE	36
	16. PRICE CODE

17. SECURITY CLASSIFICATION OF REPORT	18. SECURITY CLASSIFICATION OF THIS PAGE	19. SECURITY CLASSIFICATION OF ABSTRACT	20. LIMITATION OF ABSTRACT
UNCLASSIFIED	UNCLASSIFIED	UNCLASSIFIED	UL

INTENTIONALLY LEFT BLANK.

USER EVALUATION SHEET/CHANGE OF ADDRESS

This Laboratory undertakes a continuing effort to improve the quality of the reports it publishes. Your comments/answers to the items/questions below will aid us in our efforts.

1. ARL Report Number/Author ARL-TR-2494 (Papados) Date of Report May 2001

2. Date Report Received _____

3. Does this report satisfy a need? (Comment on purpose, related project, or other area of interest for which the report will be used.) _____

4. Specifically, how is the report being used? (Information source, design data, procedure, source of ideas, etc.) _____

5. Has the information in this report led to any quantitative savings as far as man-hours or dollars saved, operating costs avoided, or efficiencies achieved, etc? If so, please elaborate. _____

6. General Comments. What do you think should be changed to improve future reports? (Indicate changes to organization, technical content, format, etc.) _____

CURRENT ADDRESS

_____
Organization

_____
Name E-mail Name

_____
Street or P.O. Box No.

_____
City, State, Zip Code

7. If indicating a Change of Address or Address Correction, please provide the Current or Correct address above and the Old or Incorrect address below.

OLD ADDRESS

_____
Organization

_____
Name

_____
Street or P.O. Box No.

_____
City, State, Zip Code

(Remove this sheet, fold as indicated, tape closed, and mail.)

(DO NOT STAPLE)